Malkin, R., Trask, R. S., & Bond, I. P. (2013). Control of unstable crack propagation through bio-inspired interface modification. Composites Part A: Applied Science and Manufacturing, 46, 122-130. 10.1016/j.compositesa.2012.11.001

Control of unstable crack propagation through bio-inspired interface modification

Robert Malkin, Richard S. Trask, Ian P. Bond

Advanced Composites Centre for Innovation and Science

University of Bristol, England, BS8 1TR

rob.malkin@bristol.ac.uk, r.s.trask@bristol.ac.uk, i.p.bond@bristol.ac.uk

Tel: +44 (0)117 331 5311

Corresponding author: Robert Malkin - Rob.Malkin@bristol.ac.uk

Abstract

Selective toughening can be used to improve specific interfaces in a fibre reinforced polymer (FRP) component which may otherwise act as crack initiation sites. Interfacial tougheners (such as interleaves and powder treatments) have typically been deployed in a simplistic manner. However, by discretely and judiciously introducing toughening agents, taking inspiration from nature, a step change in toughness characteristics can be demonstrated. Cracks propagating through these toughened regions give rise to interesting fracture phenomena. The work presented herein shows that by incorporating regions of variable toughness, unstable crack propagation can be avoided and graceful degradation to failure demonstrated. Using both Mode I double cantilever beam testing and finite element modelling this study shows how selective toughening can be used without unstable crack growth.

Keywords:

A. Discontinuous reinforcement

A. Particle-reinforcement

B. Delamination

B. Fracture toughness

1 Introduction

Fibre reinforced polymer composite laminate interfaces can be selectively toughened to increase damage tolerance, where selective toughening is said to be "the application of a interlayer at critical locations that are potential sites for premature composite failure" [1]. Selective toughening can be applied to areas which require local toughening, such as free-edges, holes and highly stresses regions. Selective toughening has also been used to improve adhesive delamination resistance[2], as well as constraining composite delamination caused by impact loading [3]. A well known application of selective toughening is in the composite wings of the Bell Boeing V-22 Osprey [4].

Research into localised toughening began in the mid-1970's resulting in a promising outlook. For unknown reasons it was not fully developed, a situation possibly attributed to the development of increasingly tough resin systems to address the inadequacies of early systems. Much of the research into selective toughening considered the inclusion of adhesive strips between plies of pre-preg tape prior to cure [5][6][7][8][9].

Localised toughening is an alternative to global toughening as it can reduce manufacturing cost/complexity, maintain weight/dimension requirements or minimise any adverse effects of introducing toughening enhancements. While selective toughening can result in increased damage tolerance there is a consequence from its application. The concept of toughening is based on increasing critical strain energy release rate (*Gc*) over the baseline toughness. If we consider the use of an interleave material on a single ply interface, the resulting toughening is highly discretised between a region of high and low toughness, separated by a 'step' change. The consequence of this arrangement is manifest when a crack propagates across this boundary. The 'excess' strain energy released when propagating from high to low toughness will result in unstable crack jumping. Therefore, it is of interest to investigate methods where

selective toughening may still be used but without this associated problem. This work investigates a method of transforming the discrete change in toughness described above to a 'pseudo-continuous' effect, thereby promoting stable crack propagation from high to low toughness regions of a laminate interface. The design of the interface was inspired by observing the interfaces between different materials in biological structures. Such as root systems in tree's, root interface between tooth and jaw, tapered finger joints in woodwork and more specifically the interface between tissues in horse hoofs, as shown in Figure 1.

In the engineering community there are limited examples of selective toughening to control damage propagation. However, one example which has proved successful is the control of crack propagation in sandwich panels with functionally graded interior core junctions or the inclusion of sub-structural components [10][11][12][13][14].

Sandwich materials are layered structural components composed of thin strong face layers separated and bonded to light-weight (typically foam) core materials. Different core materials are often selected depending on the structural loading and level of integrity required. Due to the layered composition of sandwich structures, face–core interface delamination is a commonly observed failure mode, often referred to as peeling failure, which drastically diminishes the structural integrity of the structure. In recent years there has been a desire by the designer to ‘blend’ different core materials within the sandwich to minimize weight and maximize structural integrity in selective zones. This methodology has resulted in the formation of highly stressed tri-material regions with inherently different elastic material properties. In an effort to diminish the local failure at these junctions, the concept of ‘functionally graded’ cores, where the mechanical properties of the functionally graded cores vary gradually with the location within the material, have been investigated [11], [12]. In these investigations it was observed structurally graded core junction fatigue life was up to 30%

higher sandwich beams with the conventional junction design [12]. An alternative method for crack deflection is the inclusion of a sub-structural component embedded into the sandwich panel [11], [12]. The key purpose of this feature (see Figure 2) is to arrest face–core interface crack propagation by rerouting the crack path into a closed/restricted area of the sandwich panel, thus preventing the catastrophic failure of the sandwich structure. This approach, which utilises the available space in the through-thickness direction between the two skins, has been shown experimentally to retain at least 10% of their initial beam bending stiffness, while the conventional beams retained none [13].

The approach for selective toughening in composite sandwich panels is very unique to the geometry and material combinations employed. Whilst functionally graded core interfaces and different material combinations have been used to reroute the critical crack path, the concept of promoting stable crack propagation from high to low toughness regions of a composite laminate interface has not yet been considered. The aim of this study is to improve specific interfaces within a fibre reinforced polymer (FRP) component which may otherwise act as crack initiation sites. Ideally through discretely and judiciously introduction of toughening agents, taking inspiration from nature, unstable crack propagation can be avoided and graceful degradation of inherently brittle composite materials demonstrated.

2 Experimental Methodology

As the aim of this study was to develop a method of varying the interfacial toughness over a distance, the type of modifier was of importance. It was felt that a particulate toughener was suitable as the small particle sizes would allow the toughener to be deposited in varying densities. In essence, particulate modifiers can be applied in variable areal densities whereas film inserts are discrete in their toughening ability. A commercially available elastomer particulate, Duomod DP5045 (Zeon Chemicals LP, USA), has previously been shown to increase the interlaminar fracture toughness in carbon FRP, thus was selected for the study of interface modification [15]. The cross-linked carboxyl-functional particulate is supplied as a fine powder with a typical particulate size of 10µm.

It was observed in the early stages of the study that the amount of particulate deposited on an interface has a large effect on the fracture toughness. A relatively small deposition of the particulate would result in a toughness increase but if the interface became saturated by too much particulate the toughness would be drastically reduced. Thus, the quantity of toughener deposited was an important parameter, albeit practically challenging to control.

2.1 Experimental design

In order to asses the effect of the Duomod particulate on the interlaminar fracture behaviour Mode I double cantilever beam (DCB) testing was carried out. IM7-8552 carbon fibre/epoxy pre-preg tape (Hexcel UK) was chosen as the baseline material system. The mode I fracture properties were tested according to ASTM Standard 5528 [16]. The generic DCB specimen is shown in Figure 3.

All specimens were tested on an Instron 3343 screw driven electromechanical test machine (fitted with a 1kN load-cell) under displacement control at crack-opening displacement of

1mm/min. The location of the crack was recorded during the test using a digital video macro camera. Specimens were clamped via piano hinges attached in the fixtures. The mode I strain energy release rate (G_I) was calculated according to the modified beam theory, using Equation 1.

$$G_I = \frac{3P\delta}{2b(a+|\Delta|)} \quad (1)$$

Where; P = load, δ = crack opening displacement, b = specimen width, a = crack length and Δ = compliance correction factor. Δ is experimentally derived from a least squares regression analysis of the cube root of compliance as a function of crack length, and had a value of 0.045±0.023. An example of a DCB specimen mid-test is shown in Figure 4.

2.2 Specimen Manufacture

2.2.1 Host laminate manufacture

Unidirectional pre-preg tape was cut into 300mm x 300mm sheets. Twenty-four plies were laid up and a process of vacuum bagging applied to remove entrained air every four plies. During manufacture an insert of polytetrafluoroethylene (PTFE) film (13 µm thickness), was inserted between the 12th and 13th ply to act as a crack initiator. The laminates were cured in an autoclave according to the manufacturers recommendations [17]. Following cure of the parent laminates, specimens were cut on a diamond abrasive disc before being polished with 400/800/1200 grade SiC to minimise free edge effects. Individual DCB specimen dimensions were 140mm in length, 3.1mm in thickness and 25mm in width.

Stainless steel piano hinges were attached to the samples using Redux 810 (Hexcel, UK) epoxy adhesive [18]. In order to aid the visual identification of the crack location, the edges of DCB

specimens were spray-painted with a light coat of a brittle white paint. With accordance to the ASTM test standard no pre-crack was used on any of the tested samples.

2.2.2 Pre-preg surface modification

Specimens treated with Duomod underwent an additional manufacturing step. The amount of particulate deposited as an interlayer was controlled by using a 45µm mesh sieve (Retsch, UK). As previously mentioned the control of particulate mass deposited upon the pre-preg surface was a challenging aspect of the experimental work. The position of the deposition area was controlled with the use of the manufactured masks, these did not however allow the quantity of particulate deposited to be controlled. Normally the quantity of particulate deposited would be measured by an increase in the pre-preg mass, however given very low quantity of particulate deposited on the pre-preg surface the increase in mass was within the error of measurement of the laboratory scales available. Therefore a method of indirectly controlling the particulate mass by way of light reflection was developed. The method relied on the high reflectivity of the white DuoMod powder. Using consistent lighting and a static set-up, shown in Figure 5, the amount of particulate deposited could be inferred. Using the light meter of a single lens reflex camera, the amount of light (with reflectance increasing with increasing particulate deposited) and thus amount of particulate could be indirectly estimated. During initial testing a number of different quantities of particulate were deposited and tested to establish a suitable quantity of particulate (giving rise to a noticeable increase in fracture toughness) and therefore a corresponding reflectance from the pre-preg surface. It should be noted however that the reflectance method only works with relatively low quantities of particulate deposited upon the surface as once maximum reflection is achieved additional particulate will no longer influence reflectance.

Once a reference reflectance was established it was possible to determine if too much or too little powder had been deposited. The areal deposition was found through mass measurement to be around 2g/m^2 , which assuming a uniform interply thickness of 10µm (as measured using optical microscopy) and a measured particulate density of approximately 1780kgm^{-3} would give a volume fraction of 11%.To allow good repeatability of powder deposition onto the pre-preg surface an acrylic mask was designed and cut using a laser computer numeric control (CNC) cutting table (Hobart PLS 3.60, Hobart Lasers Ltd, UK). The dimensions which govern the design of the mask and the manufactured guide are shown in Figure 6. A transition region width of 25mm (parameter a_s in Figure 6 left) was chosen as it would allow a suitable number of crack length measurements to be taken. A 'finger' spacing (parameter b_s in Figure 6 right) of 6.25mm were chosen as it was shown to be the limit of accurate mask manufacture using the laser cutting table. Using the masking, sprinkling and reflectance technique outlined above, it was possible to repeatedly treat the pre-preg with the requisite amount of powder deposited in the correct location.

2.3 Specimen Description

Four specimen designs, labelled as designs [A]-[D], were tested. The plan view of the interfaces between the 12th-13th plies (the interface for the specimen delamination) are shown in Figure 7. For configurations A & B, the toughening agent was simply applied to separate regions. In both cases, PTFE film was used to mask off portions of the pre-preg surface with would not be treated. For configurations C&D the particulate was deposited using the mask as a guide. The exposed regions were then treated with the Duomod powder as discussed above. Figure 8 shows example surfaces after being treated with Duomod particulate in both discrete (upper figure) and continuous (lower figure) regimes. The four specimen designs,[A]-[D], allow assessment of mode I interlaminar crack propagation of discrete and graded/continuous changes in fracture toughness.

3 Experimental Results

3.1 Specimen types A & B

All specimens of type A [low to high discrete toughness step] showed similar responses. With the initiation of the crack at the end of the initiator film, the crack propagated steadily between the plies. Once the crack approached the boundary of the toughened region the crack began to slow. The crack was arrested until the load was increased sufficiently to allow propagation through the toughened region until the samples were fully delaminated. During testing no crack jumping was observed.

As with type A, all type B [high to low discrete toughness step] specimens showed the same initial experimental response. The initial crack growth in toughened IM7-8552 was steady with no crack jumping observed. However, once the crack had travelled approximately 30mm (to the boundary between toughened and untreated IM7-8552) the crack propagated very rapidly (<0.1 seconds). The unsteady delamination was accompanied by a large load drop. After sufficient crack opening displacement the crack began to propagate further until the sample was fully delaminated.

For all specimens of type A & B, mode I initiation and propagation strain energy release rate G_I values were calculated in accordance with ASTM Standard 5528 for the first 30mm of crack growth in both untreated and toughened IM7-8552 and are shown in Table 1. Resistance curves for specimen types A and B are shown in Figure 9.

3.2 Specimen types C & D

Type C [low to high continuous toughness step] specimens all showed similar responses. The crack initiated and propagated along the first 30mm. By observing a local increase in the crack opening load it could be inferred that the crack was now propagating into the higher

toughness transition region. The crack propagated across the transition region into the toughened IM7-8552 interface with no crack arrest or jumping.

Type D [high to low continuous toughness step] specimens all showed similar responses. The crack would initiate at the end of the crack initiation film and propagate steadily to the start of the transition region. The crack would then propagate smoothly across the transition region with no visible jumping or load drops. Once the crack had cleared the transition region it propagated in unmodified IM7-8552 interface until the sample was fully delaminated. The resistance curves for type C and D specimens are shown in Figure 10.

3.3 Discussion of experimental results

Discrete changes in toughness, as seen in configurations A and B, result in some interesting fracture mechanics. For configuration A, little crack jumping is evident with temporary crack arrest at the low to high toughness interface. The opposite scenario is seen for configuration B, which highlights the significant problem of unstable crack growth often found with the introduction of selective toughening. Once the crack propagates into a region of lower toughness the excess strain energy results in rapid delamination. This is clearly seen in Figure 9, which shows an absence of measurable G_c values, once the crack had propagated beyond the edge of the high toughness region to approximately 15mm into the low toughness region where the crack length could again be accurately measured. With a graded change in interfacial toughness (as used in configurations C and D), unstable crack growth can be inhibited. Configuration C shows that crack propagation from low to high toughness does not create any instability. However, configuration D indicates that the unstable rapid delamination, observed in configuration B, can be avoided by using a 'graded' interface region. In order to help understand the delamination process exhibited by the 'graded' transition region, implicit finite element analysis(FEA) modelling was undertaken.

4 FEA modelling

The aim of the modelling was to investigate how an inter-ply delamination behaved as it traversed the graded region. DCB specimen configurations [C] and [D] were modelled, where;

- Model 1 - Configuration C: Low to high $G_{propagation}$ continuous transition.
- Model 2 - Configuration D: High to low $G_{propagation}$ continuous transition.

4.1 Model details

Modelling was conducted using Abaqus CAE 6.10-2. The DCB model is shown in Figure 11 and is based upon the DCB specimens tested experimentally, the only significant difference being the piano hinges being replaced with a line at which the crack opening displacement was applied. The interlayer region shape was taken to be identical to those tested experimentally. The model was allowed to run until the specimen had fully delaminated. Given the relatively large geometric deformations exhibited by the the DCB model, geometric nonlinearities (where deformation effects stiffness) were accounted for by using the NLGEOM (also known as large deformation analysis) modelling option within Abaqus.

4.1.1 Composite beam section

The FEA model was based on the experimental samples with dimensions of 25mm width, 140mm length and 3.1mm thickness. The beam sections were assigned 3D brick elements with linear order and anisotropic material properties given in Table 2. For individual cantilever sections the thickness (1.55mm) was modelled using 8 elements. The total number of elements for each individual cantilever was 10,816.

4.1.2 Interlayer section

The crack insert was simply modelled by having no cohesive elements in the first 50mm of the specimen, as per experimental specimens. The interlayer region was partitioned into two

regions according to the shape of the mask as shown in Figure 8. In order to mitigate numerical difficulties caused by the sharp corners of the mask, as observed during preliminary modelling, the triangular partitions in the model had slightly blunted corners as shown in Figure 12.

A cohesive element approach was used to model the interfacial region with a traction-separation constitutive law. The values of fracture toughness were taken from experimental work. As is no data available in the literature for the non-physical interfacial strength, σ, of the DuoMod modified interface the values were derived from curve fitting. Experimental and FEA load-displacement data were simultaneously plotted, with σ varied until FEA and experimental curves were indistinguishable. Other values were taken from literature, as shown in Table 3.

The size of the cohesive zone, defined as "the distance from the crack top to the point where the maximum cohesive traction is attained" [19], was estimated to be 0.84mm for the baseline interface and 1.30mm for the Duomod treated interface. The cohesive zone length was estimated using the formulation found in [20], and is shown in Equation 2.

$$l_{cohesive} = \frac{EG_c}{(\sigma_{Model})^2} \tag{2}$$

where E is taken as the transverse modulus, E_{22} .

Different suggestions for the number of elements required to span the cohesive zone can be found in the literature [21][22][23]. Given the geometry of the transition region contained relatively sharp triangular features the mesh density required to suitably mesh the region was higher than the suggested mesh density. The size of the cohesive elements was chosen as 0.2mm giving between 5 ~ 7 elements to span the cohesive zones of the baseline and Duomod

interfaces, respectively. This exceeds the suggested value of 4 cohesive elements for the cohesive zone as found in [19].

For all cohesive models, viscous regularisation was used to aid convergence with a value of $1x10^{-8}$ s used, as taken from literature modelling DCB failure [19]. As the geometry of the cohesive interfaces in the presented work are non-trivial, four further models were tested. Models 3, 4, 5 and 6 are based on Model 2 (High to low toughness change), but with an increased mesh density. These models are summarised in Table 4. The purpose of models 3-6 was to asses the 'resolution' of model 2. In essence, these variants act to perform a mesh sensitivity study with the aim being to ensure that the cohesive zone was insensitive to further refinement to the mesh density.

Models 3-6 only consider the scenario of high to low toughness transition, the reason being that a crack propagating under these circumstances, across a boundary of discrete toughness change, would conventionally result in an unstable crack and as such, this was thought to be a more interesting study to pursue.

5 FEA results

5.1 Models 1 & 2

Load-displacement curves from both Models 1 & 2 are shown in Figure 13. Models 1 & 2 are both based on cohesive elements with a general size of 0.2mm. The delamination growth can be illustrated by plotting the cohesive element damage scalar, or SDEG, as used by other authors [24]. The SDEG has a value between 0 and 1, where 0 represents an undamaged element and 1 a fully failed element. In Figure 14 the SDEG value is shown with the delamination approximately half-way across the transition region. In both the low-to-high and high-to-low scenarios the crack front appears smooth with no indication that the change in fracture toughness is affecting the crack front shape.

5.2 Models 3-6

Models 3-6 have an increased mesh density which show a very different crack propagation profile to that observed in Model 2. All models show an irregular crack front due to the fracture toughness difference across the interface. The SDEG plots for models 3 & 6 are visually indistinguishable, therefore, it can be assumed that a greater refinement in the mesh would not result in any greater insights into the crack front shape. Using the same method as above, the SDEG values are shown for a number of different crack lengths for model 3 in Figure 15.

5.3 Discussion of FEA results

The increasing mesh density in models 3-6 resolve details which would be missed if the cohesive zone size formulation discussed in 4.1.2 were used. This suggests that non-trivial cohesive zones need careful meshing. A note of importance is that the load-displacement

curves for models 2-6 are almost identical, therefore, care needs to be taken to ensure that for complex interfaces the cohesive zone is sufficiently meshed.

The staggered crack front seen in Figure 15 suggests an explanation for the steady crack propagation observed experimentally (as shown in Figure 10). It appears that there are effectively two distinct crack fronts propagating simultaneously but at different 'rates', in each of the low and high toughness regions. The low toughness crack appears to lead of the high toughness by around 1mm. This uneven crack front suggests that the high toughness region 'retards' the low toughness region from unstable propagation across the entire transition region.

6 Conclusions

The work presented has shown that a commercially available DuoMod interface toughening agent can increase the mode I fracture toughness in IM7-8552 by 34% for crack initiation and 55% for crack propagation, it can also be used to maintain steady crack propagation. Typically, a crack propagating from high to low interfacial toughness will become unsteady by virtue of excess residual strain energy, however, this can be mitigated by grading the interface and thus selectively toughening.. Finite element modelling of the interfacial failure has shown that a graded interface results in a complex crack profile and suggests that the strain energy release rate is variable along the crack front (as suggested by the periodic crack profile). The grading of the interface can be thought of as a means of averaging the strain energy release rate over the transition region resulting in smoother crack propagation.

While the work presented investigated rubber particulate toughness modification it is felt that a similar design methodology could be used with properly implemented toughening mechanisms, such as film interleaving and through thickness reinforcement such a z-pinning.

Future work on this topic would investigate the effect of different transition region geometries and the corresponding effect on delamination response. The current work presents a number of variables which could be modelled numerically to investigate the possibility of optimal transition regions. In addition to this it would be of interest to see how the continuous transition methodology discussed in the present work could be integrated into damage contamination principles currently being explored [3].

7 Acknowledgements

The authors kindly acknowledge; Rolls Royce PLC and Great Western Research for funding the research, Ian Chorley and Simon Chilton for help with sample preparation, Julie Etches for assistance with mechanical testing, and Prof Chris Pollitt for the kind use of Figure 1.

8 References

[1] O. Ishai and N. Sela, “Interlaminar Fracture Toughness and Toughening of Laminated Composite Materials:,” *A Review, Composites*, vol. 20, no. 5, pp. 423-435, 1989.

[2] E. Sancaktar and S. Kumar, “Selective use of rubber toughening to optimize lap-joint strength,” *Journal of Adhesion Science and Technology*, vol. 14, no. 10, pp. 1265-1296, Jan. 2000.

[3] M. Yasaee, I. P. Bond, R. S. Trask, and E. S. Greenhalgh, “Damage control using discrete thermoplastic film inserts,” *Composites Part A: Applied Science and Manufacturing*, vol. 43, no. 6, pp. 978-989, Jun. 2012.

[4] “Bell Pushes for Broader Applications Of Composites to Helicopter Structures,” *Aviation Week & Space Technology, 126 (1987)*, pp. 95-96.

[5] W. S. Chan, C. Rodgers, and S. Aker, “Improvement of Edge Delamination Strength of Composite Laminates Using Adhesive Layers,” in *Composite Materials: Testing and Design (Seventh Conference)*, 1986, pp. 266-285.

[6] W. S. Chan, *Composite Materials: Fatigue and Fracture*. 100 Barr Harbor Drive, PO Box C700, West Conshohocken, PA 19428-2959: ASTM International, 1986, pp. 176-196.

[7] T. L. Norman and C. T. Sun, “Delamination growth in composite laminates with adhesive strips subjected to static and impact loading,” *Composites Science and Technology*, vol. 46, no. 3, pp. 203-211, Jan. 1993.

[8] C. T. Sun and T. L. Norman, “Design of a laminated composite with controlled-damage concept,” *Composites Science and Technology*, vol. 39, no. 4, pp. 327-340, Jan. 1990.

[9] N. Bhatia, *Fracture Mechanics of Composites*. 100 Barr Harbor Drive, PO Box C700, West Conshohocken, PA 19428-2959: ASTM International, 1975, pp. 200-214.

[10] O. T. Thomsen, E. Bozhevolnaya, and A. Lyckegaard, “Structurally graded core junctions in sandwich elements,” *Composites Part A: Applied Science and Manufacturing*, vol. 36, no. 10, pp. 1397-1411, Oct. 2005.

[11] E. Bozhevolnaya and O. T. Thomsen, “Structurally graded core junctions in sandwich beams: quasi static loading conditions,” *Composite Structures*, vol. 70, no. 1, pp. 1-11, Aug. 2005.

[12] E. Bozhevolnaya and O. T. Thomsen, “Structurally graded core junctions in sandwich beams: fatigue loading conditions,” *Composite Structures*, vol. 70, no. 1, pp. 12-23, Aug. 2005.

[13] J. Jakobsen, E. Bozhevolnaya, and O. T. Thomsen, “New peel stopper concept for sandwich structures,” *Composites Science and Technology*, vol. 67, no. 15–16, pp. 3378-3385, Dec. 2007.

[14] J. Jakobsen, J. H. Andreasen, and O. T. Thomsen, “Crack deflection by core junctions in sandwich structures,” *Engineering Fracture Mechanics*, vol. 76, no. 14, pp. 2135-2147, Sep. 2009.

[15] E. N. Gilbert, B. S. Hayes, and J. C. Seferis, “Interlayer toughened unidirectional carbon prepreg systems: effect of preformed particle morphology,” *Science*, vol. 34, pp. 245-252, 2003.

[16] ASTM, “Standard Test Method for Mode I Interlaminar Fracture Toughness of Unidirectional Fiber-Reinforced Polymer Matrix Composites 1,” *Annual Book of ASTM Standards*, vol. 01, no. Reapproved 2007, 2008.

[17] Hexcel, “Hexcel - HexPly 8552 Epoxy: Product Data,” 2008. [Online]. Available: http://www.hexcel.com/Resources/DataSheets/Prepreg-Data-Sheets/8552_eu.pdf.

[18] Hexcel, “Hexcel - Redux 810: Product Data,” 2010. [Online]. Available: http://www.hexcel.com/Resources/DataSheets/Adhesives-Data-Sheets/810_eu.pdf.

[19] A. Turon, C. Davila, P. Camanho, and J. Costa, “An engineering solution for mesh size effects in the simulation of delamination using cohesive zone models,” *Engineering Fracture Mechanics*, vol. 74, no. 10, pp. 1665-1682, Jul. 2007.

[20] A. Hillerborg, M. Modéer, and P.-E. Petersson, “Analysis of crack formation and crack growth in concrete by means of fracture mechanics and finite elements,” *Cement and Concrete Research*, vol. 6, no. 6, pp. 773-781, Nov. 1976.

[21] N. Moës, “Extended finite element method for cohesive crack growth,” *Engineering Fracture Mechanics*, vol. 69, no. 7, pp. 813-833, May 2002.

[22] M. L. Falk, A. Needleman, and J. R. Rice, “A critical evaluation of cohesive zone models of dynamic fractur,” *Le Journal de Physique IV*, vol. 11, no. PR5, pp. Pr5-43-Pr5-50, Sep. 2001.

[23] C. Davila, P. Camanho, and M. de Moura, “Mixed-Mode decohesion elements for analyses of progressive delamination,” in *42nd AIAA/ASME/ASCE/AHS/ASC Structures, Structural Dynamics and Materials Conference - Seattle*, 2001.

[24] B. Chen, P. Wu, and H. Gao, “Geometry- and velocity-constrained cohesive zones and mixed-mode fracture/adhesion energy of interfaces with periodic cohesive interactions,” *Proceedings of the Royal Society A: Mathematical, Physical and Engineering Sciences*, vol. –1, no. –1, p. -1--1, Jan. 2009.

[25] J. Scho, T. Nyman, A. Blom, and H. Ansell, “A numerical and experimental investigation of delamination behaviour in the DCB specimen,” *Composites Science and Technology*, vol. 60, pp. 173-184, 2000.

[26] A. Turon, P. P. Camanho, J. Costa, and J. Renart, “Accurate simulation of delamination growth under mixed-mode loading using cohesive elements: Definition of interlaminar strengths and elastic stiffness,” *Composite Structures*, vol. 92, no. 8, pp. 1857-1864, Jul. 2010.

[27] P. P. Camanho, C. G. Davila, and M. F. De Moura, “Numerical Simulation of Mixed-Mode Progressive Delamination in Composite Materials,” *Journal of Composite Materials*, vol. 37, no. 16, pp. 1415-1438, Jan. 2003.

9 Figures

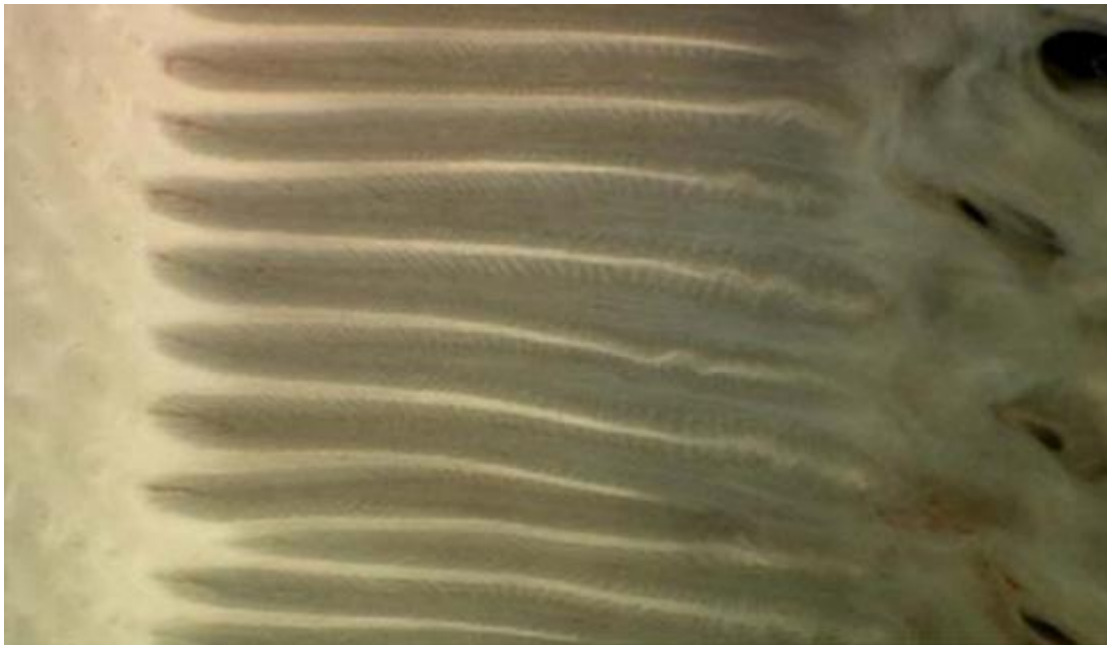

Figure 1 - Interface between high toughness (left) and low toughness (right) epidermal layers of horse hoof showing interdigitated transition region, image courtesy of Dr Chris Pollitt, University of Queensland.

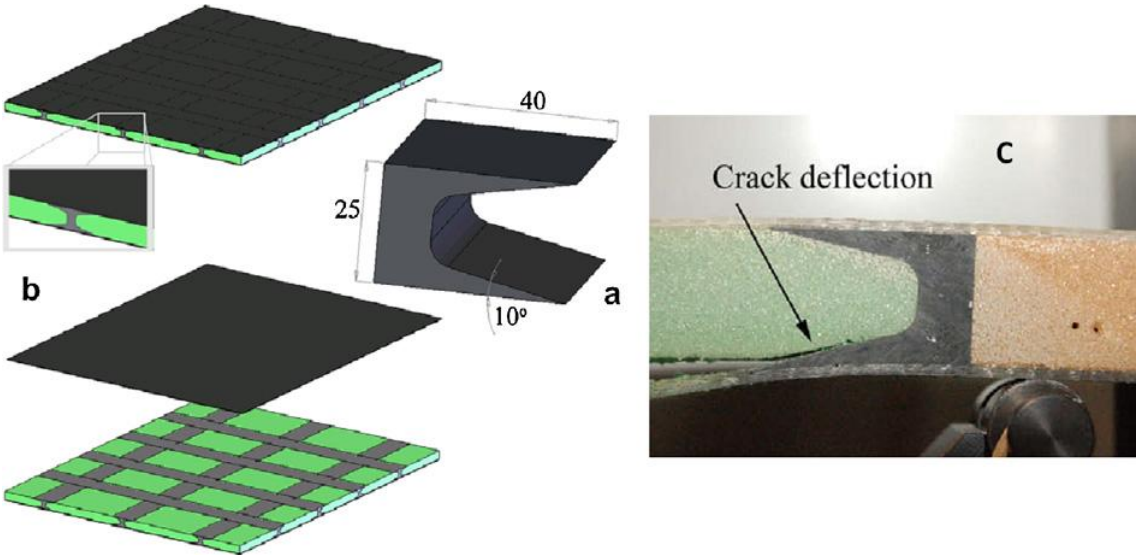

Figure 2 - Proposed design of the peel stopper[13] (a). The case shown displays a crack rerouting angle of 10°. A suggested implementation of the proposed peel stoppers in a sandwich plate is shown in (b) where the grid type pattern will confine damage to the grid mesh. (c) photo of a peel stopper has been embedded between the two foam cores. The wedge of the peel stopper deflects the interface crack into the core, where the crack was finally arrested and thereby confining the delamination propagation[14].

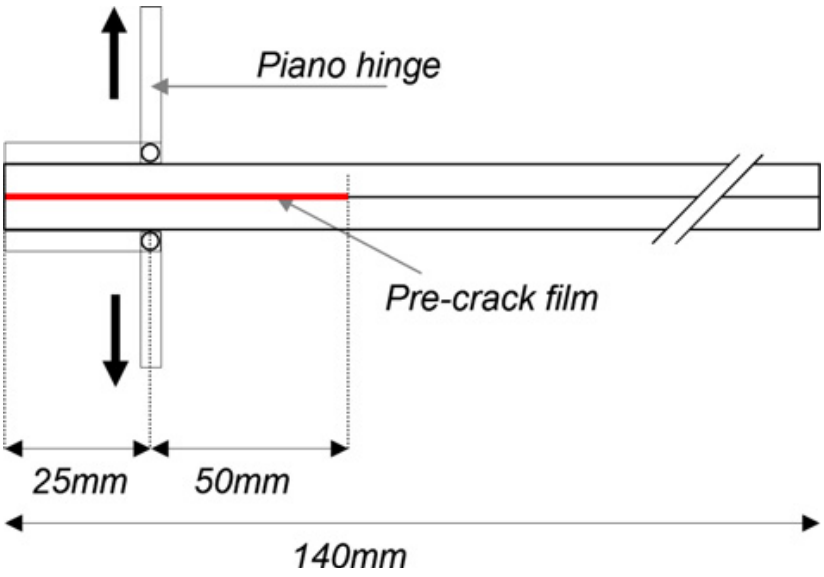

Figure 3 - Schematic of generic DCB specimen.

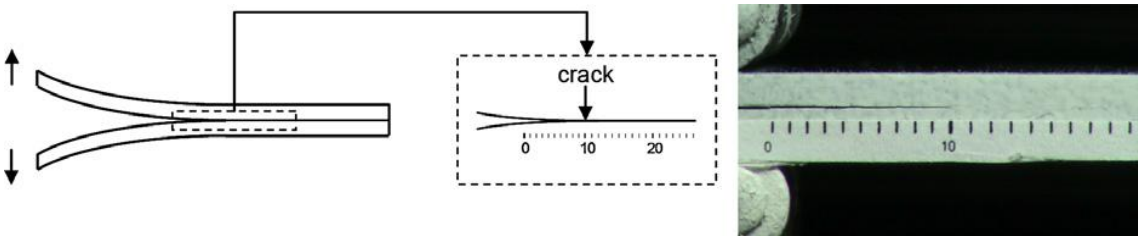

Figure 4 - Left: DCB specimen showing location of crack edge. Right: Video still image of crack position mid-test.

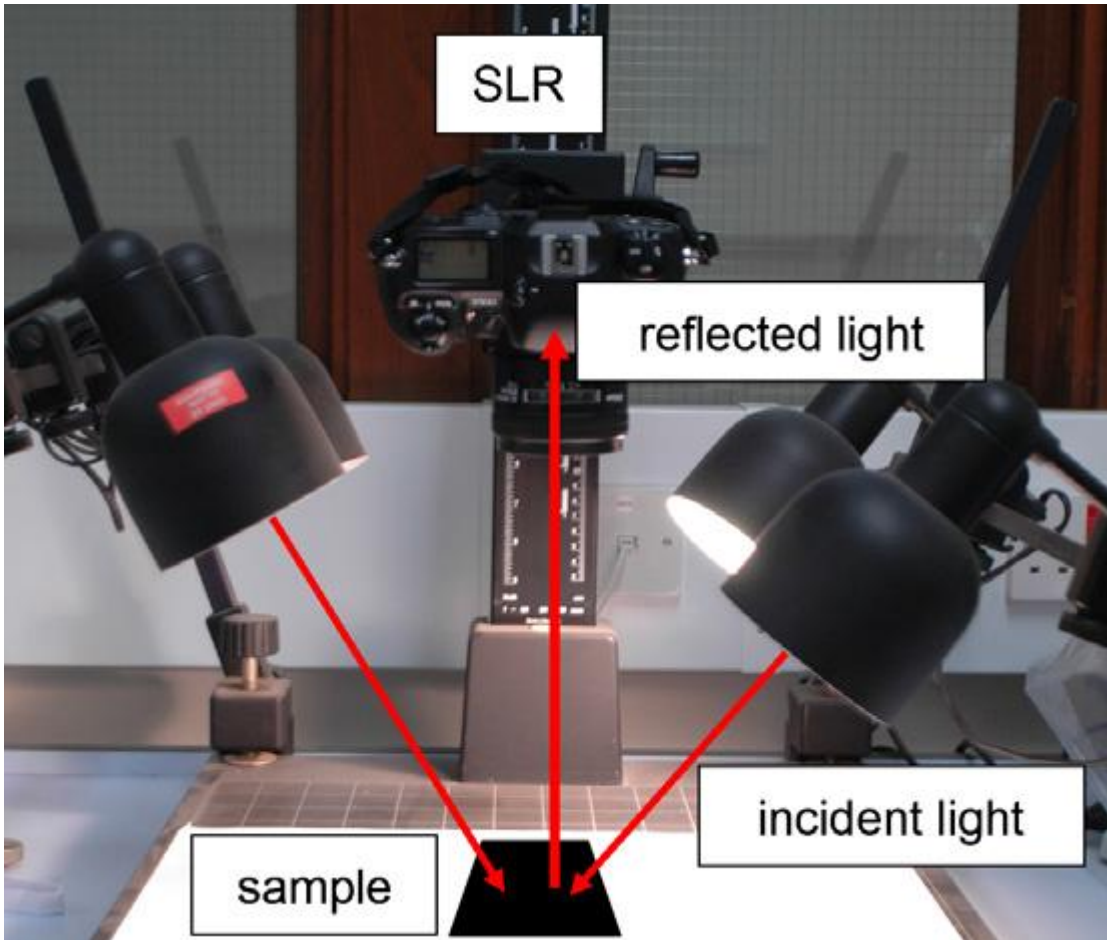

Figure 5 - Reflectance method used to determine when the desired amount of Duomod had been deposited onto the pre-preg surface. (Unsymmetrical lighting sources used to ensure even lighting distribution on surface.)

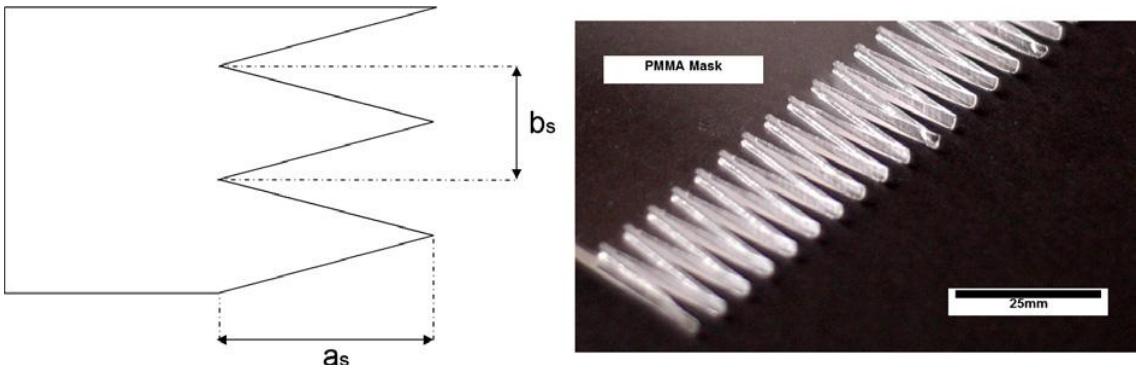

Figure 6 - Left: design parameters. Where as governs the length of the transition region and bs controls the 'finger' spacing of the transition. Right : Manufactured acrylic mask with dimensions of as=25mm and bs=6.25mm.

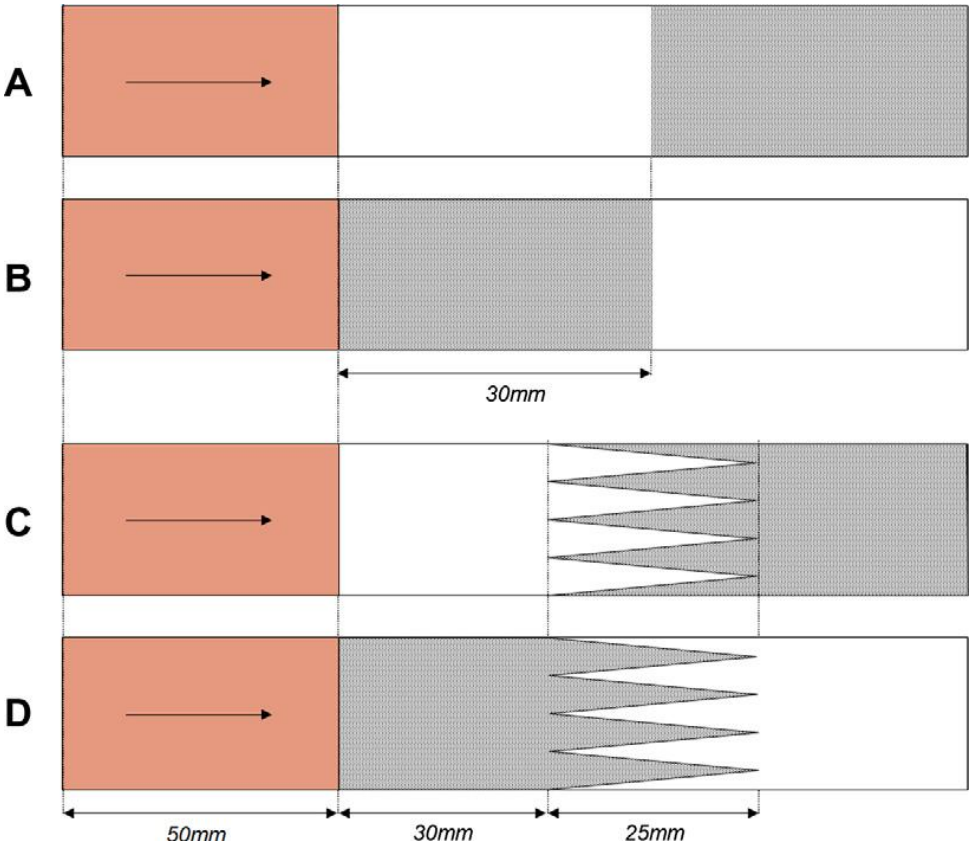

Figure 7 - Schematics of interface configurations tested. [A]&[B] show discrete toughening profiles and [C]&[D] show graded profiles. Orange regions show the location of the PTFE pre-crack and the direction of the crack growth. The white regions are unmodified pre-preg.

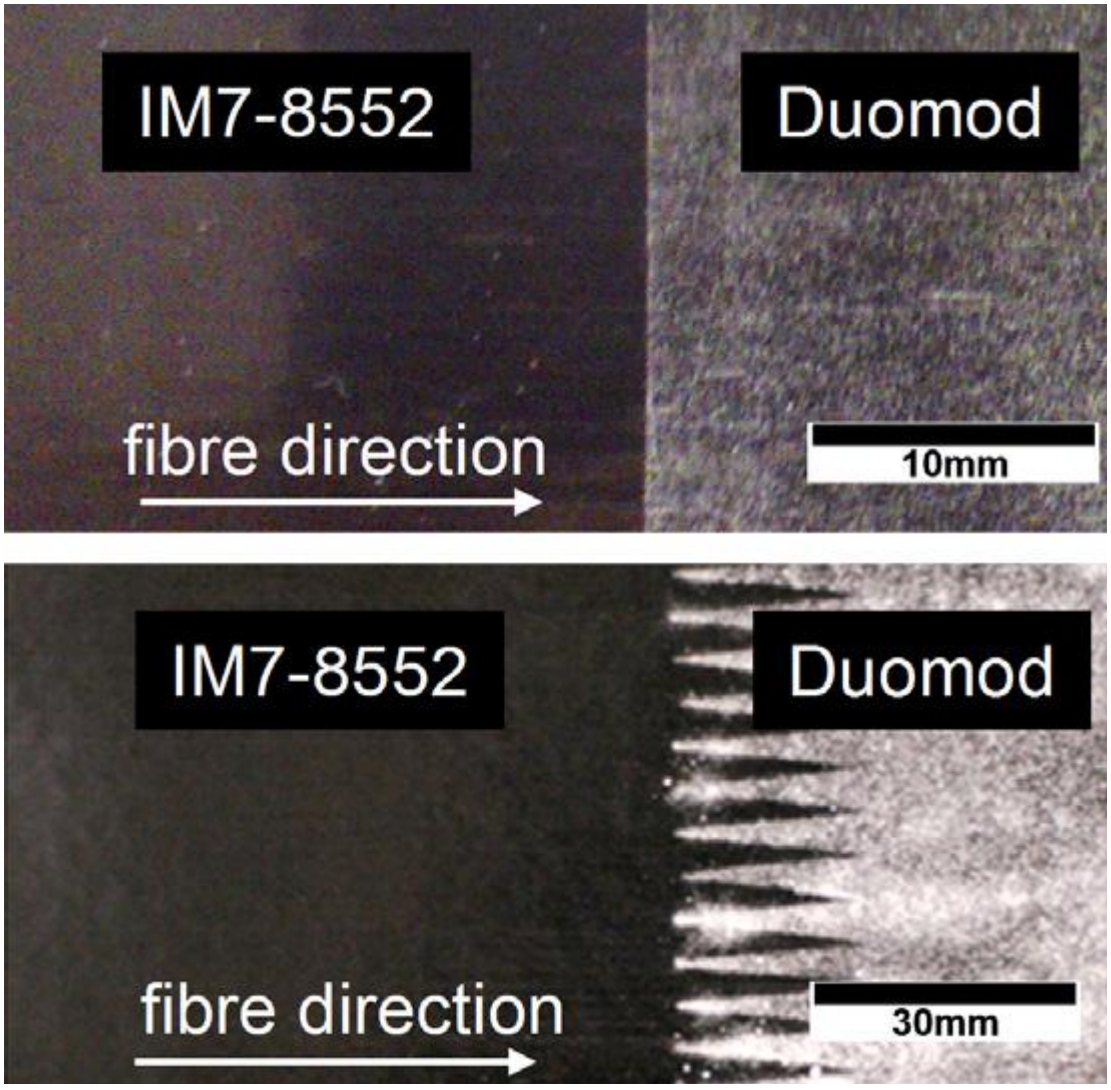

Figure 8 - Duomod modified IM7-8552 pre-preg surfaces. Upper: Discrete toughness transition design. Lower: 'Shaded' toughness transition design.

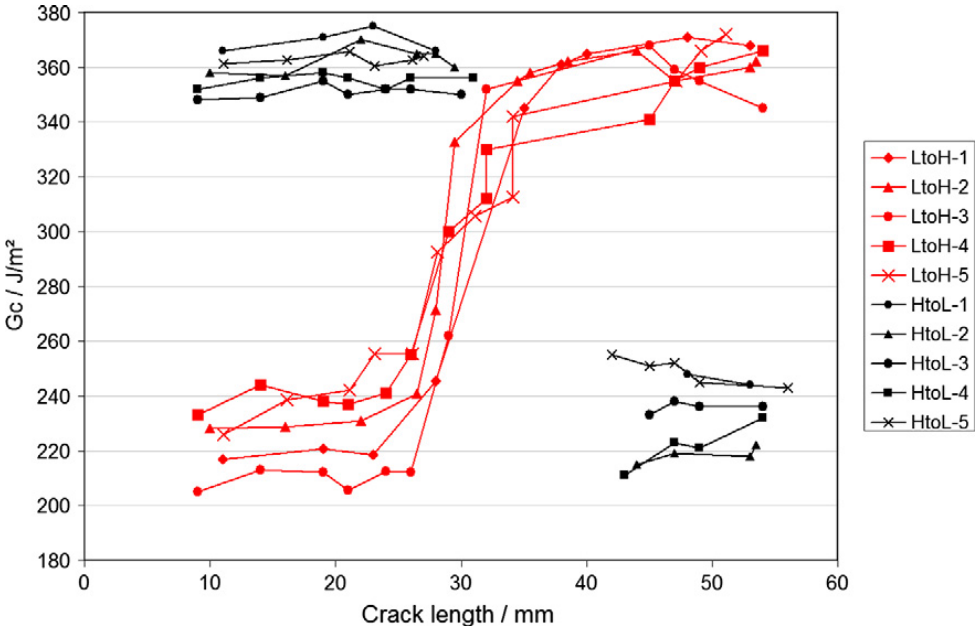

Figure 9 - Resistance curves of crack propagation across discrete toughening boundary for specimen types A+B. LtoH: Low to High. HtoL: High to Low.

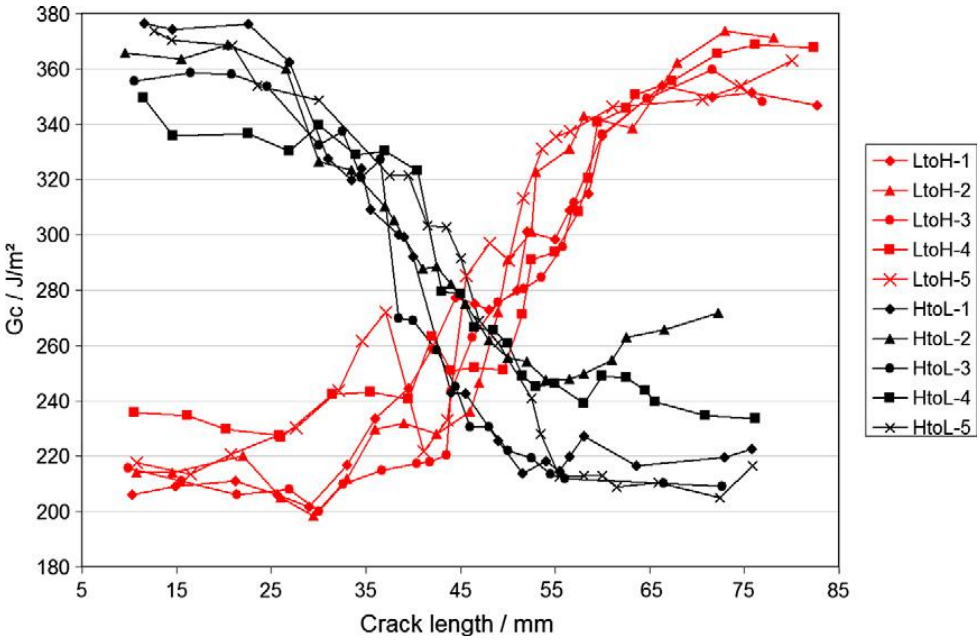

Figure 10 - Resistance curve of crack propagation across continuous toughening boundary for specimen types C+D. LtoH: Low to High. HtoL: High to Low.

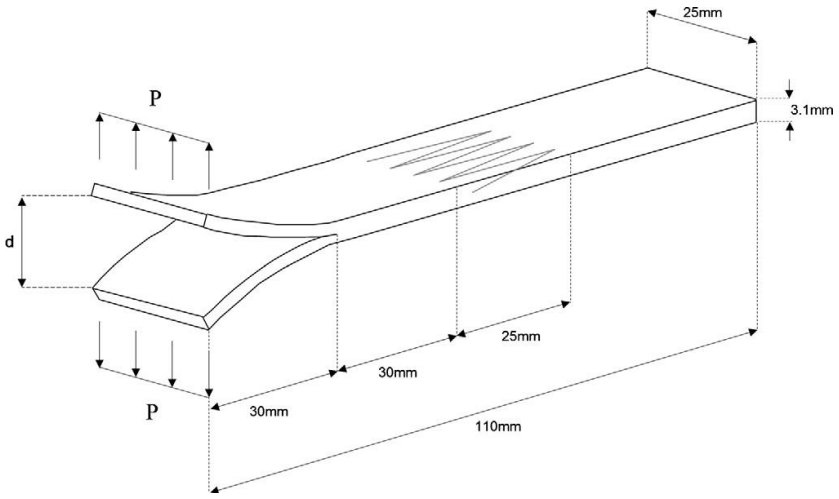

Figure 11 - Schematic of DCB model. P, applied edge load, d, crack opening displacement. The transitional region of the interface is shown midway through the thickness of the specimen.

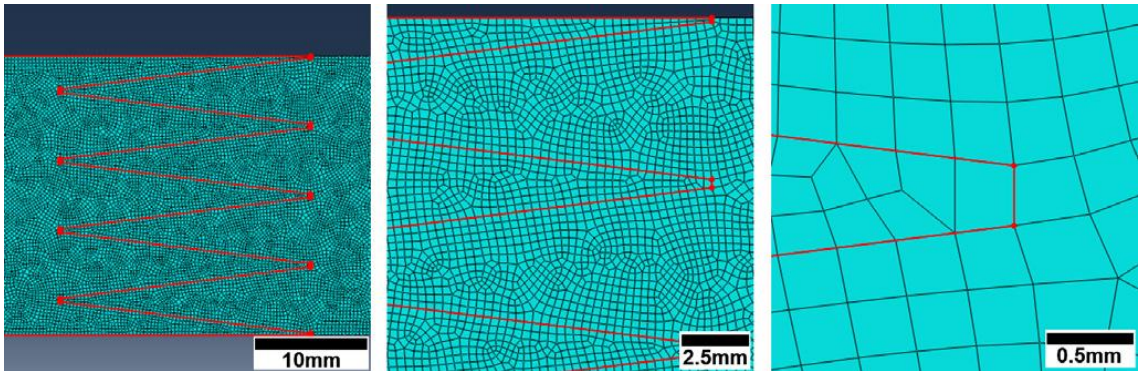

Figure 12 - Plan view of example mesh of interlayer region at increasing magnification, showing triangular separated regions and truncated corner (highest magnification).

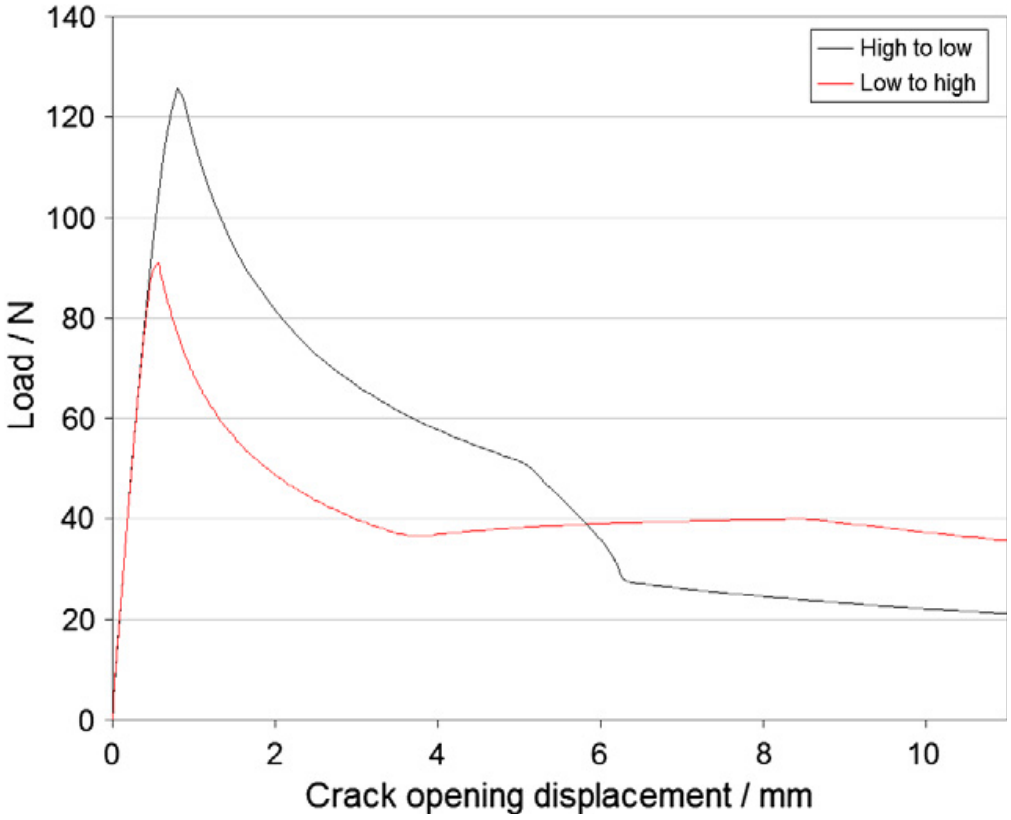

Figure 13 - Load-displacement curves for model 1 (low to high toughness) and model 2 (high to low toughness).

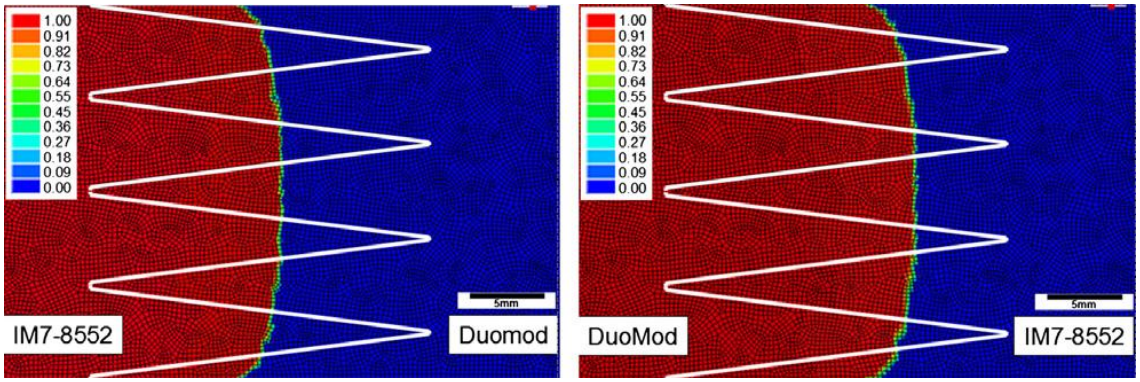

Figure 14 - SDEG value representation of crack front for models 1 (left) and 2 (right).

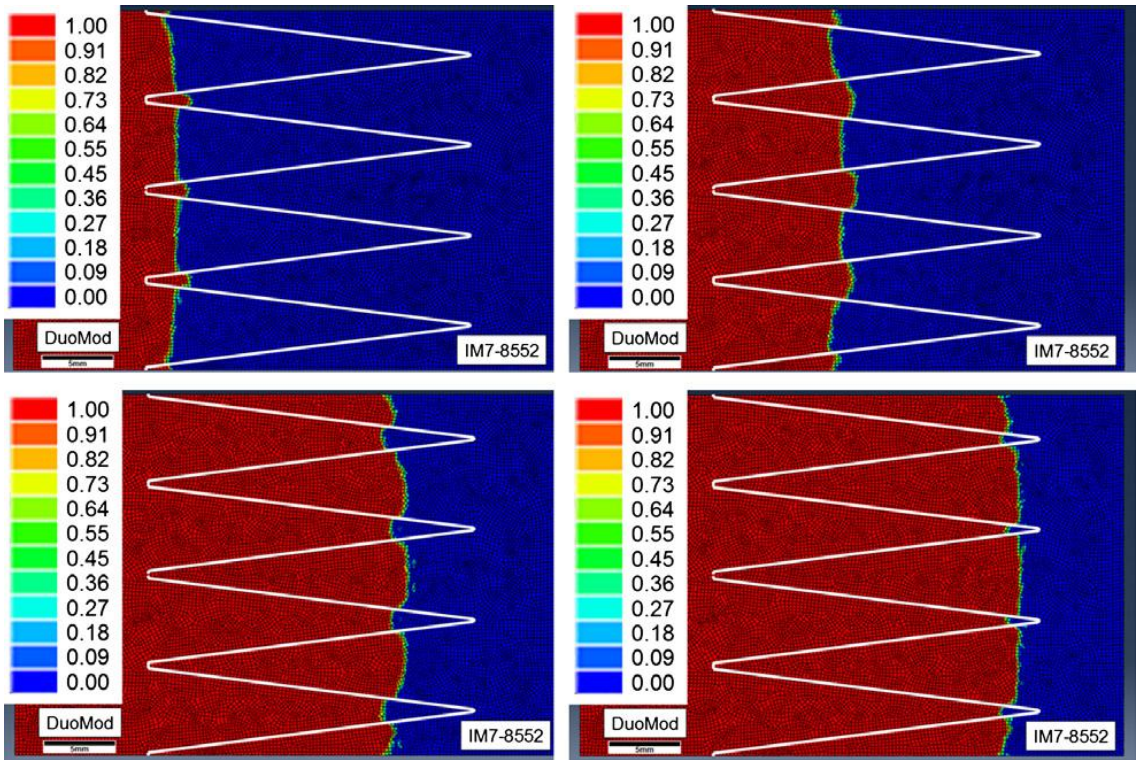

Figure 15 - SDEG value representation of crack front of model 4 at different crack propagation lengths.

Tables

Table 1 - Mode I Initiation and propagation toughness values (*GIc*) for unmodified and toughened IM7-8552. Standard deviations are given in parentheses.

G_{IC} - J/m²	Baseline	DuoMod	Increase / %
Initiation	280 (35)	374 (52)	34
Propagation	233 (27)	361 (31)	55

Table 2- Material properties for 3D solid elements of IM7-8552 for FEA [25]**.**

E_{11} = 160 GPa	E_{22} = 13 GPa	E_{33}=13 GPa
G_{12} = 4.8 GPa	G_{13} = 4.8 GPa	G_{23}= 3.2 GPa
V_{12} = 0.31	V_{13} = 0.31	V_{23} = 0.52

Table 3 - Material properties for cohesive elements of IM7-8552 and DuoMod interface for FEA (GC values from experiment, others [19], [26], [27]**).**

$K_1 = 1x10^6$ N/mm³	$K_2 = 1x10^6$ N/mm³	$K_3 = 1x10^6$ N/mm³
$\sigma_{mode\ I}$[IM7-8552] = 60 MPa	$\sigma_{mode\ II}$[IM7-8552] = 90 MPa	$\sigma_{mode\ III}$ IM7-8552] = 90 MPa
$\sigma_{mode\ I}$[DuoMod] = 152 MPa	$\sigma_{mode\ II}$[DuoMod] = 152 MPa	$\sigma_{mode\ III}$[DuoMod] = 152 MPa
$G_{IC-IM7-8552} = 233$ Jmm^{-2}	$G_{IIC-IM7-8552} = 986$ Jmm^{-2}	$G_{IIIC-IM7-8552} = 986$ Jmm^{-2}
$G_{IC\ -\ DuoMod} = 361$ Jm^{-2}	$G_{IIC\ -\ DuoMod} = 1821$ Jm^{-2}	$G_{IIIC\ -\ DuoMod} = 1821$ Jm^{-2}

Table 4 - Mesh density details of models 1-4. Model 1 - low to high transition, Models 2,3,4 high to low transition.

Model	General cohesive element size	General solid element size	No. of cohesive elements, interface	No. of solid elements, each cantilever	No. of elements for whole DCB model
1 & 2	0.20mm	0.80mm	55k	11k	77k
3	0.15mm	0.60mm	65k	28k	122k
4	0.10mm	0.40mm	96k	83k	262k
5	0.05mm	0.20mm	127k	142k	412k
6	0.025mm	0.10mm	143k	167k	478k